PCCP

Molecular-Scale Understanding of Diluent Effects on Ligand Assembly for Metal Ion Separations

Journal:	*Physical Chemistry Chemical Physics*
Manuscript ID	CP-ART-12-2023-005972.R2
Article Type:	Paper
Date Submitted by the Author:	11-Mar-2024
Complete List of Authors:	Poe, Derrick; Argonne National Laboratory, Chemical Sciences and Engineering Division Seifert, Sönke; Argonne National Laboratory, X-ray Science Division Servis, Michael; Argonne National Laboratory,

PCCP

ARTICLE TYPE

Cite this: DOI: 00.0000/xxxxxxxxxx

Molecular-Scale Understanding of Diluent Effects on Ligand Assembly for Metal Ion Separations†

Derrick Poe,*[a] Soenke Seifert,[b] and Michael J. Servis*[a]

Received Date
Accepted Date

DOI: 00.0000/xxxxxxxxxx

Use of metal-selective ligands in solvent extraction is instrumental in critical material extraction and recycling, yet diluent effects on extraction performance is not well understood. Experimental and empirical solvent parameters have been proposed to correlate with extraction performance, but are often inadequate predictors. We follow the hypothesis that the diluents' primary influence on extraction efficiency is in enabling or hindering assembly the bulky extracting ligands in solution into a geometry necessary for metal complexation. This behavior is readily accessible with molecular dynamics (MD), where the atomistic description of molecules can be applied to arbitrary extractant–solvent molecules and their mixtures. Several simulated quantities are considered, from both pairwise or graph theoretic analyses, and compared to experimental distribution ratio data for americium extraction by TODGA in a series of inert, non-interacting diluents. These simple properties, especially the formation of closed triplets corresponding to the 3:1 ligand:metal stoichiometric solvate, suggest potential predictive power of this approach. This methodology provides a path forward to comprehensively understand and predict diluent effects in more complex systems involving different extracting ligands and multi-component diluent mixtures.

1 Introduction

Rare earth elements (REEs), actinides, and other metals are critical materials for modern technology, becoming increasingly more important with rapid advancements in electronics and green technologies.[1–5] It follows that separation, refinement, and purification of these metals are equally essential. The difficulty lies in the fact that feeds for these critical materials can be extremely dilute, highly acidic, have many mixed competing ions, or combinations of all three.[6–8] Liquid–liquid extraction (LLE), or solvent extraction, is naturally suited to selectively partitioning these aqueous target species into an immiscible organic phase with energy costs significantly lower than that of other separations methods.[9–12] While classic solvent extraction methods simply select specific solvent mixtures to achieve this goal, modern techniques facilitate extraction and generate selectivity between ions through the use of complex ligands designed to preferentially and selectively bind target metal ions and enhance organic-phase partitioning.[11,13] Extraction efficiency is typically quantified by a distribution ratio,

$$D_M = \frac{[M]_{org}}{[M]_{aq}} \tag{1}$$

where D_M is the ratio of concentrations of the metal ion in the organic extractant phase to the aqueous phase.

In efforts to enhance extraction performance, the extractant ligand often receives a high degree of study,[14–18] and rightfully so considering their intricacy and the expansive design-space. However, the extractant is diluted by an organic solvent, called the diluent, that improves the physical properties (e.g., viscosity) of the organic phase. The impact of the diluent on metal extraction is significant, where the same extractant ligand can possess orders of magnitude difference in its distribution ratio simply by changing the diluent.[19,20] While these so-called diluent effects have been historically reported,[21,22] modern studies frequently focus on ligand design. Attempts to explain these diluent effects have been made using experimental or empirical solvent descriptors such as dielectric constants,[23] solubility parameters[24] or diluent parameters.[21] These relationships are often uncorrelated and not motivated from a fundamental, molecular-level understanding, limiting their predictive capability. For example, one might expect a higher dielectric constant of the diluent to enhance solubility of polar metal-containing species, while in fact the opposite is often the case.[25] This inconsistent behavior of diluent effects confounds the rational choice of diluent for a target system, ne-

---

[a] Chemical Sciences and Engineering Division, Argonne National Laboratory, Lemont, IL 60439, USA.
[b] X-ray Science Division, Argonne National Laboratory, Lemont, IL 60439, USA.
Email: dpoe@anl.gov; mservis@anl.gov

† Electronic Supplementary Information (ESI) available: Discussion of fractal dimensionality and additional figures and tables. Also included are necessary GROMACS files to replicate the MD simulations. See DOI: 10.1039/cXCP00000x/

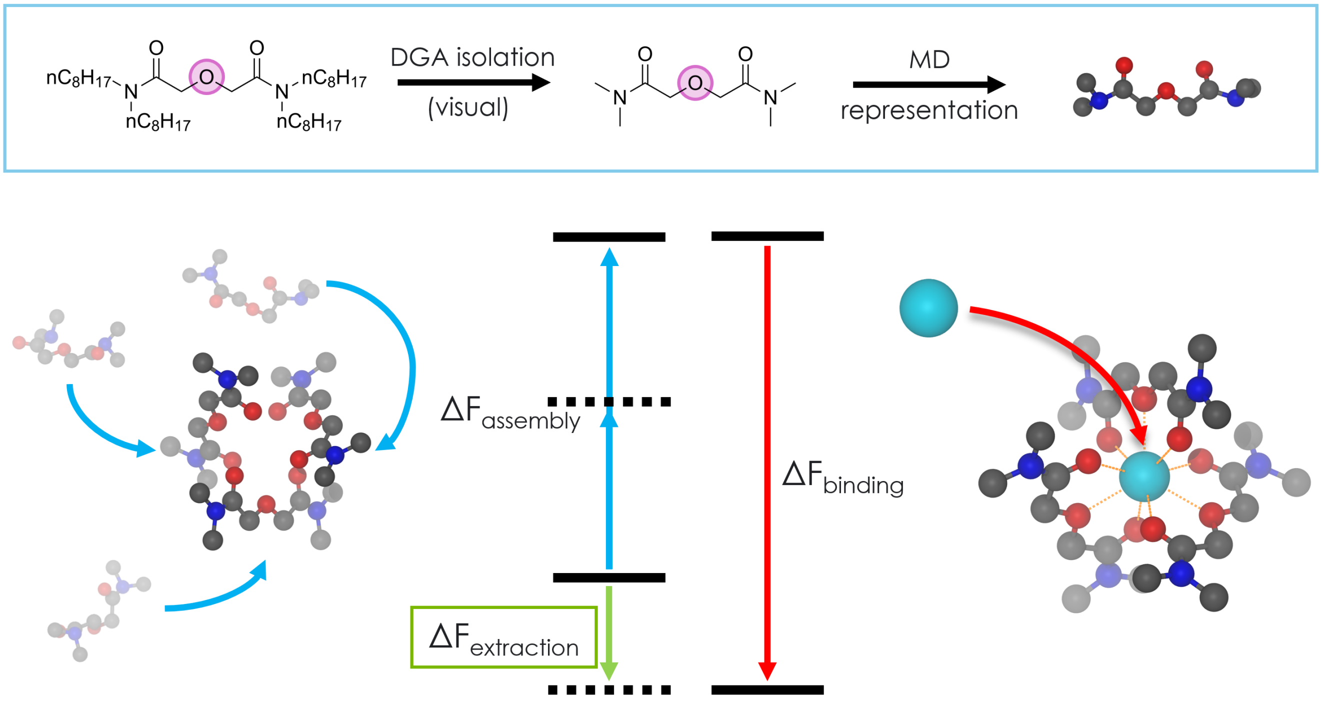

Fig. 1 Top: Explanation of TODGA visual representation for this study. Octyl tails are excluded for clarity, and the central etheric oxygen (O_c), used in later analysis, is highlighted in pink. Bottom: Free energy diagram of solvent extraction processes. On the left is the positive $\Delta F_{assembly}$ process of TODGA trimer assembly, split in two to represent a DGA dimer and subsequent trimer assembly. On the right is a depiction of the negative $\Delta F_{binding}$ process of metal–ligand complexation. The final energy difference $\Delta F_{extraction}$ provides the chemical gradient driving solvent extraction. Relative ΔF arrow lengths are not necessarily to scale, and charge-balancing ions and TODGA octyl tails are omitted for clarity.

cessitating simple, physically motivated explanations.

The importance of diluent effects has been known of since the 1960s when Healy demonstrated that even different "inert diluents" — diluents that do not directly participate in the extracted complex — can increase or decrease distribution ratios by orders of magnitude.[26] While aliphatic diluents typically enable significantly better extraction than aromatic solvents, studies by Regadío *et al.* found that mixed diluents with both aliphatic and aromatic components performed only slightly worse than the pure aliphatic mixtures.[27] This suggests that diluent effects are complex and nonlinear, indicating that empirical approaches such as solubility parameters derived from mixing rules[28] are not sufficient to capture actual behavior. Poirot *et al.* examined solvent effects from the perspective of solvent structuring and the resultant effect on energetics. They found that weak solvent interactions induced pre-organization of malonamide aggregates and affected trivalent Nd extraction more than divalent Pd, driving up both distribution ratios and Nd selectivity.[29] Finally, most diluent studies are focused on screening solvents to maximize distribution ratios rather than understanding solvent effects from a molecular level, which, while practically useful, does little to develop a holistic understanding of diluent effects.

It is important to recall that solvent extraction is fundamentally driven by differences in solvation free energies, where the final extracted species yields a lower free energy than the initial species present either in the aqueous phase (water-solvated target metal ions) or solvent phase (free ligands). An overall idea of the energy differences in this process is illustrated in Figure 1. Complexation of a REE ion with ligands is typically highly enthalpically favorable, and when calculated computationally yields a large negative energy of complexation, $\Delta F_{complex}$.[30–33] What is not captured by this approach are positive ΔF contributions that can counteract the complexation favorability, a critical one being assembly of ligands into a complex favorable for ion coordination, which necessarily occurs within a diluent. This is the $\Delta F_{assembly}$ seen in Figure 1, which we hypothesize is highly sensitive to diluent choice and is the primary mechanism by which inert diluents affect separations energetics. There exists an energy penalty for organizing these bulky molecules into a binding configuration, and that penalty can differ from solvent to solvent. By focusing on minimizing this assembly energy, more efficient extraction of target metals can be achieved without needing to improve metal–ligand binding behavior. Note that because the extraction free energies are state functions, the final determinant of distribution ratio is the overall $\Delta F_{extraction}$ rather than any specific mechanism or assembly path. This approach is also more tractable than involving all potential solvent extraction species, as only binary ligand-in-solvent systems need to be studied. With this approach, understanding how ligands behave in the purely ligand-in-solvent system and the changes in $\Delta F_{assembly}$ on $\Delta F_{extraction}$ would contribute greatly in understanding this final energy difference.

To study diluent effects on extractant assembly, a ligand of sufficient complexity was chosen as a representative test case, specifically *N,N,N',N'*-tetraoctyl diglycolamide (TODGA). DGAs have a strong affinity for trivalent ions, making them particularly useful for extraction of lanthanides and minor actinides.[18,25,34–36] To validate the idea that TODGA self-association is a critical driver of diluent effects, four initial test solvents of n-hexane, n-dodecane, benzene, and toluene were chosen. It is emphasized that these solvents are non-interacting and known to not alter or participate in the metal–ligand extraction complex, i.e., they are inert diluents in this extraction system. In these cases, three TODGA molecules extract target trivalent metals, which is useful since it emphasizes complexation energetic effects on extraction more-so than a dimer or monomer extracting complex such as TEHDGA or ADAAM-EH, respectively.[37] Distribution ratios of americium, D_{Am}, in these solvents from Ansari *et al.* were used as a self-consistent dataset of metal extraction.[25] With these selected systems, it can be demonstrated in Figure 2 how dielectric constant, diluent parameter, nor solubility parameter entirely correlate with D_{Am} in these four solvents. Furthermore, Figure 2d includes a correlation plot for dielectric constant of all solvents reported in Ansari *et al.*, demonstrating how extremely poorly dielectric constant more broadly correlates with D_{Am}.

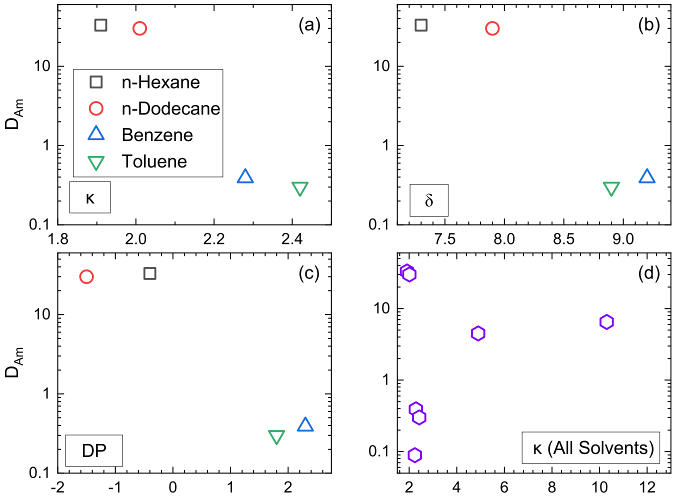

Fig. 2 Comparison of the log of D_{Am} with solvent (a) dielectric constant, (b) solubility parameter, and (c) diluent parameter in n-dodecane, n-hexane, benzene, and toluene. Included in (d) is a dielectric constant comparison for all solvents included in Ansari *et al.*.[25]

In order to fully understand ligand–diluent assembly and structuring, TODGA behavior at both the molecular level and nanometer length-scale is needed. Molecular dynamics (MD) is well suited for this task, capable of extracting system-level output such as density or SAXS patterns as well as providing molecular-level resolution of ligand assembly that is traditionally difficult to achieve experimentally. MD simulations have proven useful for providing understanding of TODGA solvent complexation, extraction, and selectivity in a variety of diluents and extraction systems.[38–46] By modeling TODGA in the above four solvents, while keeping in mind the framework described in Figure 1, ligand self-association and the resultant effects on energetics and liquid structure can be not only described, but meaningfully quantified. This study proposes that intuitive quantities derived from MD simulations of binary ligand–solvent mixtures, absent of any metal, can serve as a better predictor of diluent effects on distribution ratios than previously proposed experimental descriptors. These simulations can also provide insight into the molecular interactions that effect such large extraction differences. Finally, by being based on MD simulations using general-purpose force fields, this approach is inherently generalizable and highly expandable to new ligands, solvents, or solvent mixtures of interest in future studies of diluent effects.

2 Methodology

2.1 Small Angle X-ray Scattering

SAXS measurements were performed at beamline 12-ID-C[47] at the Advanced Photon Source (APS). *N*,*N*,*N*′,*N*′-tetraoctyldiglycolamide (TODGA, $>99\%$ purity by HPLC) was purchased from Technocomm Ltd. and *n*-dodecane ($>99\%$ purity) was purchased from Sigma-Aldrich. Samples were prepared by massing TODGA followed by volumetric dilution with dodecane, which were then loaded into a 2 mm outer diameter quartz capillary with a remote access auto sampler. SAXS patterns were taken using a Pilatus 2M detector with a 2.133 m sample-to-detector distance and 18 keV incident x-ray energy. The SAXS pattern of each sample were averaged over five one-second exposures, followed by empty capillary subtraction and normalization to an absolute scale using scattering from pure (18 MΩ) water.[48]

2.2 Molecular Dynamics and Density Functional Theory Simulations

Atomistic classical molecular dynamics simulations were conducted using GROMACS 2022.1[49]. Fixed atomic charges and flexible bonds, angles, and dihedrals were used to describe the system described by the GAFF class 1 force field.[50] Force field parameters and charges for dodecane were taken from Vo *et al.*,[51] while n-hexane, benzene, toluene, and TODGA from the GAFF2 force field, which is an improved and ongoing update to the traditional GAFF force field. Partial charges for TODGA were fit by performing vacuum phase density functional theory (DFT) optimization on a single molecule with Gaussian16[52] at the B3LYP/6-311++G level of theory and basis set[53,54] followed by AM1-BCC[55] fitting of the optimized conformation with Antechamber.[56] Additional DFT analysis was performed of N,N,N',N'-tetramethyl diglycolamide (TMDGA) monomers, dimers, and trimers in implicit solvent polarizable continuum model (PCM). Geometry optimizations of one, two, and three TMDGA molecules were each conducted using n-hexane, n-dodecane, benzene, and toluene implicit solvents, in addition to in vacuum, using B3LYP/6-31G*.

Systems were assembled by calculating the necessary number of TODGA solute molecules to achieve the target concentration within a 100 Å cubic box and subtracting off the predicted contributed volume based on density. The number of solvent molecules was determined from the remaining box volume and experimental solvent density. This resulted in systems with molecule compositions detailed in Table 1.

These molecule counts were then packed into an approximately 110 Å cubic box using Packmol version 17.333.[57]. The

Table 1 System compositions

Solvent	[TODGA] (mM)	Solvent Molecules	TODGA Molecules
n-Hexane	200	3991	120
Benzene	200	5889	120
Toluene	200	4941	120
n-Dodecane	100	2482	60
n-Dodecane	200	2312	120
n-Dodecane	300	2139	181
n-Dodecane	400	1970	241
n-Dodecane	500	1800	301
n-Dodecane	600	1630	361
pure TODGA	1560	0	937

packed systems were energy minimized using a steepest descent algorithm with a threshold of 300 kJ $\mathrm{mol^{-1}nm^{-1}}$ and step size of 0.001 nm. The minimized system was equilibrated in the isothermal-isobaric ensemble (NPT) at 300 K and 1 atm with a 2 fs timestep, stochastic velocity rescaling thermostat with a 0.2 ps time constant, and a Berendsen barostat with a 2 ps time constant. The resultant equilibrated system was then fed into a canonical (NVT) ensemble at 300 K held at the final system volume of the NPT trajectory using a Nosé-Hoover thermostat and time constant of 0.4 ps. The NVT system was equilibrated for 10 ns before continuing into a 100 ns production run for data collection. Both NPT and NVT simulations utilized a timestep of 2 fs, a cutoff of 15 Å for van der Waals and coulombic interactions, and a Particle-Mesh Ewald solver for long-range electrostatics. A linear constraint solver (LINCS) restraint was imposed on all hydrogens bound to heavy atoms, fixing the bond length at the equilibrium bond length.

Radial distribution functions (g(r)), structure factors (S(q)), and spatial distribution functions (SDF) were calculated using the TRAVIS package.[58,59] S(q) was then used to calculate intensity factors (I(q)) for comparison with experiments by adding the molecular fraction weighted self-scattering following procedure detailed in Liu *et al.*[60] Graph theoretic analysis was performed with the NetworkX python package.[61] Snapshot and SDFs were rendered using both Ovito[62] and VMD.[63]

3 Results and Discussion

3.1 Model Validation

Validation of the MD model is critical to extract accurate physical insight from the *in silico* systems. Densities of the pure components, shown in Table 2 were accurately captured compared to experimental values,[64–68] with a largest deviation of 4.7% with n-dodecane and the rest at 2% or less error. Given the focus on structure of this study, further validation of the MD model tied to liquid structure was performed by comparing experimental and simulated SAXS patterns.

X-ray scattering patterns, and structure factors more broadly, provide detailed information of structural patterns in a system with a broad length-scale range from first-solvation sphere effects all the way up to long-range structural features or fluctuations. SAXS is an important validation method for this study as it captures both short and long-range solvent structuring features, particularly TODGA aggregation occurring at the nanoscale. The presented experimental SAXS captures a q-range of of 0.02 to 0.9 $\mathrm{Å^{-1}}$, while simulated results assess ordering from the atomic scale up to approximately 50 Å, or $q > 0.13$ $\mathrm{Å^{-1}}$. This leaves considerable overlap to validate the MD model, seen in Figure 3, where SAXS scans of increasing concentrations of TODGA in n-dodecane where simulated intensity factors, $I(q)$, show good agreement between the two methods.

Table 2 Simulated and Experimental density comparison

	ρ (Exp) 298 K	Extrapolated ρ (Exp) at 300 K	ρ (Sim) 300 K	% Error
TODGA	0.9011	0.8997	0.9038	0.454
n-Hexane	0.6551	0.6528	0.6533	0.070
n-Dodecane	0.7452	0.7437	0.7789	4.729
Benzene	0.8731	0.8709	0.8899	2.176
Toluene	0.8621	0.8603	0.8736	1.554

As additional TODGA is added to the system, an ordering prepeak induced by TODGA addition grows in at approximately q = 0.3 $\mathrm{Å^{-1}}$ in both experiments and simulations. There can also be seen an increase in the extrapolated low-q $\mathrm{I_0}$ for both systems. Not only is the overall concentration trend well-captured via MD, but there is even good quantitative agreement between the two at lengthscales that are often difficult to accurately model for fully atomistic simulations. Overall, agreement with the experimental structural features at all accessible lengthscales indicates these simulations can be leveraged to understand TODGA clustering behavior with molecular-level insight.

3.2 TODGA Self-Association

An understanding of the two-order-of-magnitude difference in D_{Am} seen between aliphatic solvents n-hexane and n-dodecane compared to aromatic solvents benzene and toluene is the initial goal of this solvent effects study. With the proposed free energy framework shown in Figure 1, understanding differences in TODGA self-assembly between solvents is essential to understanding solvent effects. This self-structuring be captured by standard MD pairwise analyses. Given that the DGA group of TODGA is the functional extractant substructure, the central etheric oxygen ($\mathrm{O_c}$) of TODGA is used as the reference site for all TODGA molecules and the $\mathrm{O_c}$–$\mathrm{O_c}$ pair is the primary focus of all pairwise analyses, starting with a radial distribution function (RDF), or g(r).

Varied concentrations of TODGA in n-dodecane were first studied to ensure that the methodology is robust and extensible to reasonable concentrations of ligand in solvent. The $\mathrm{O_c}$–$\mathrm{O_c}$ pair was observed in n-dodecane in 100 mM increments from 100 mM to 600 mM TODGA. As seen in Figure 4a, the DGA structuring behavior stays effectively the same across all concentrations, exhibited by no change in the overall RDF shape, only the intensities. Primary peak positioning and lack of strong anticorrelation past the first solvation shell is preserved with increasing solute, with an overall diminishing in RDF peak intensities. There are also two key features of the primary peak, with a large initial peak centered at approximately 4.5 Å and a second, broader peak or shoulder at 7 Å.

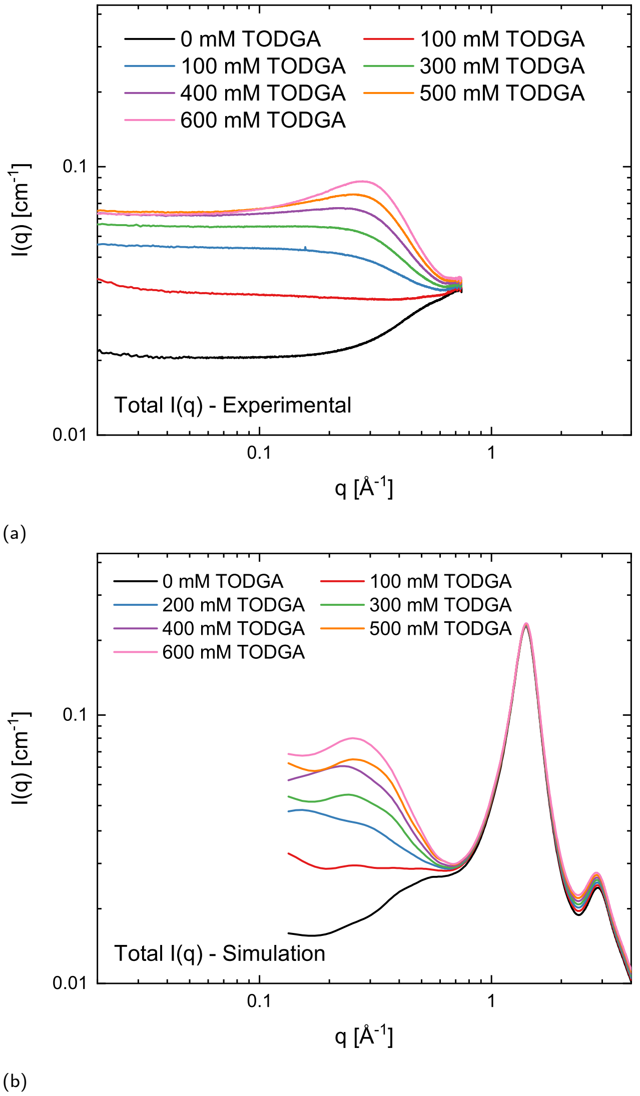

(a)

(b)

Fig. 3 SAXS patterns of 0 to 600 mM TODGA in n-dodecane with (a) experimental and (b) simulated results.

Given that RDFs are sensitive to particle density normalization, coordination numbers (N_C) can quantitatively state whether the local environment is truly changing. Figure 4b, which is N_C plotted for all concentrations, reveals that coordination number stays approximately equal up to 6 Å for all concentrations over 100 mM, implying that, on average, the same number of O_c groups coordinating any given O_c observed. This is likely simply due to the volume of space occupied by the rest of the DGA group, and indicates that the RDF peak reduction is entirely a concentration normalization effect and has nothing to do with a reduction in O_c–O_c structuring. Longer range coordination number trends seen in Figure S1 exhibit standard, homogenous concentration trends. At 100 mM, there appears to be some less counts of O_c–O_c pairs for the first solvation shell, indicating that 200 mM TODGA in dodecane is necessary to to fully saturate the pairwise interaction and maximize TODGA extraction efficiency.

The TODGA self-association can also be expressed as a free energy term $w(r)$, derived from the RDF via $w(r) = -kT\ln(g(r))$, as shown in Figures S3 and 5b. Examination of the $w(r)$ of TODGA association as a concentration effect, Figure S3, indicates that the reduction in primary peak structuring results in a shallower energy well at 4.5 Å though the overall modest energy barrier at 15 Å does not appreciably change. This can be interpreted that with an increased availability of TODGA in the immediate vicinity, there is a greater ability for any given O_c–O_c pair to disassociate either to cluster with or be displaced by a new DGA group.

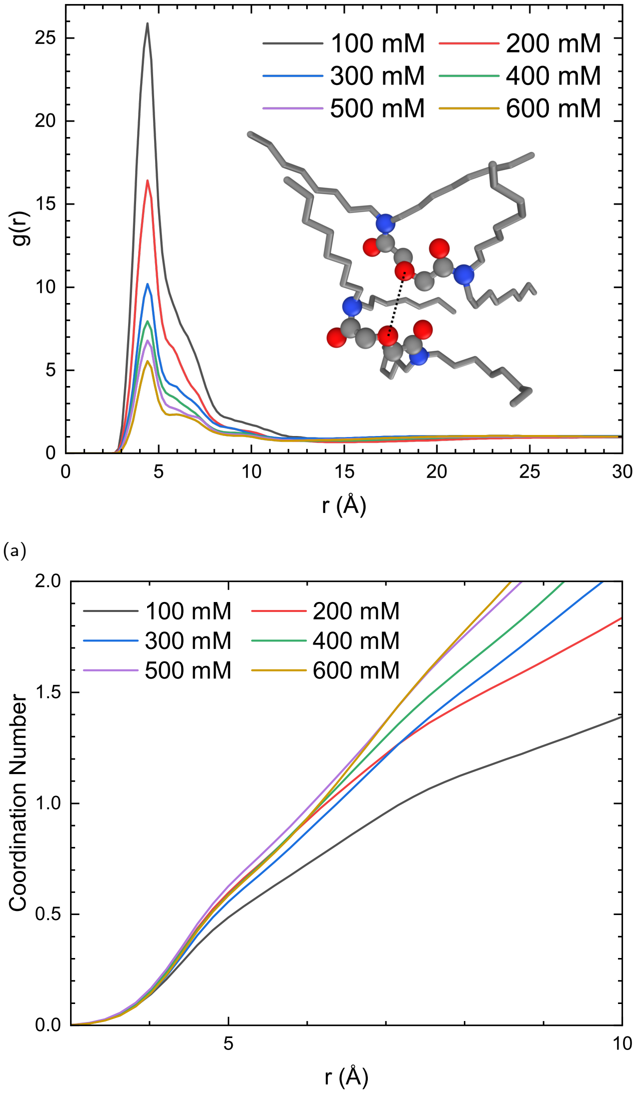

(a)

(b)

Fig. 4 Concentration effects on TODGA etheric-oxygen structuring in n-dodecane. Shown is the radial distribution function (a) and the coordination number (b) of the O_c–O_c pair.

With an understanding of solvent-extraction-relevant concentrations of TODGA in a well understood system, n-dodecane, the focus is shifted towards the main goal of understanding solvent effects on TODGA self-association. Looking at the RDF for O_c–O_c at 200 mM TODGA in the four different solvents, Figure 5a, it can be seen that TODGA maintains both the primary 4.5 Å and secondary 7 Å peaks for all solvents. While position of the first maximum the same between all solvents, implying similar first solvation structuring of TODGA, aromatic mixtures display drastically weaker structuring compared to alkanes along with anticorrelation of TODGA pairs between 6 and 20 Å. Examining the free energy transformation of g(r), a deep potential well for the alkanes of the order -2.5 kT implies a strongly favorable and unhindered association for TODGA. Conversely, the aromatic solvents indicate a minimal preference for association, -0.9 kT. There is also a notable energy barrier for benzene and toluene starting at 8 Å, though hexane has effectively no barrier. The energy barrier at long-distance for n-dodecane at 15 Å is due to anti-correlations in the g(r), likely from long-lived, statistically unlikely structures given the lack of such anti-correlation at any other concentration in Figure 4a. While not high enough to block association, the energy barriers and minimal energy well combine to imply low favorability of short-range TODGA association in aromatic solvents, while the large energy well for dodecane and hexane indicate an energetically preferred interaction.

The DGA association energies can also be estimated from gas-phase DFT using implicit solvent models. *abinitio* methods have been used to great effect for analyzing molecule pairs or small-scale, pre-defined clusters, including studies of TODGA complexes energetics in a variety of applications.[30,69–76] Use of PCM solvent models also provides an opportunity to compare results from DFT with implicit solvent to molecular dynamics modeling with explicit solvent and sampling solution-phase ensembles of associating DGA monomers. Energetic analysis of TMDGA monomers, dimers, and trimers are shown in Table 3, which is the per-molecule energy change of TMDGA going from a monomer to a dimer or trimer in their respective solvents. These are calculated using $\Delta E = E_N^{solvent}/N - E_1^{solvent}$. Tetra-methyl functionalized DGA was used instead of tetra-octyl to model DGA interaction behavior while maintaining computational feasibility. These demonstrated that the ΔE for a TMDGA molecule to form a dimer or trimer is negative in vacuum and all four solvents. However, DFT calculations did not properly group the energy differences into different groupings for aliphatic and aromatic solvents, with benzene exhibiting the greatest multimer formation favorability. Looking at total system energies in Table S1, subtracting off vacuum system energies to better compare each system to each other similarly shows a lack of the experimental trend. Potential explanations for the DFT approach not resulting in the correct experimental trends are: 1) sampling ensembles of clusters, rather than single energy-minimized structure at zero temperature, would be necessary to accurately represent condensed phase behavior, or 2) the implicit solvent model does not account for aspects of the solvent energetics, such as cavitation energies of the solvent itself, which we hypothesize is a dominant component of DGA assembly energy. This effect would be significantly more unfavorable in aromatic solvents, explaining why it is not captured in this DFT approach but is adequately captured with the explicit solvent MD method.

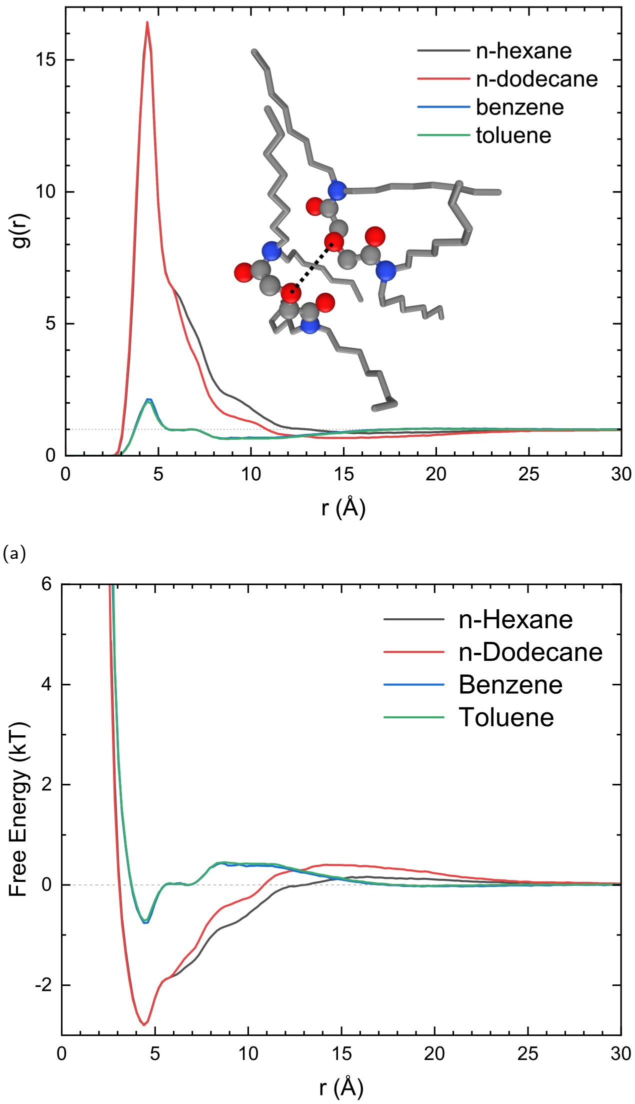

(a)

(b)

Fig. 5 Radial distribution function between etheric oxygens of TODGA molecules in various solvents and the free energy of the pair calculated via $w(r) = -kT\ln[g(r)]$.

A link between these TODGA–TODGA pairwise associations with distribution ratios from a traditional solvent extraction framing can be demonstrated with equilibrium constants using Figure 1 as a guideline. The overall extraction complex formation can be written as:

$$3\,\overline{\text{TODGA}} + \text{M} \xrightleftharpoons{K_{ex}} \overline{\text{TODGA}_3\text{M}} \tag{2}$$

where we use M to represent a neutral trivalent metal-anion salt, such as nitrate salts of actinides or lanthanides ($\text{An(NO}_3)_3$ or $\text{Ln(NO}_3)_3$). Overbars indicate organic phase species. We decompose this process into two independent steps:

$$3\,\overline{\text{TODGA}} \xrightleftharpoons{K_T} \overline{\text{TODGA}_3} \tag{3}$$

$$\overline{\text{TODGA}_3} + \text{M} \xrightleftharpoons{K_M} \overline{\text{TODGA}_3\text{M}} \tag{4}$$

where Equation 3 is the formation of a hypothetical TODGA trimer in the metal-binding configuration. The next step, given in Equation 4, is complexation of the metal by the hypothetical preformed TODGA trimer, which we assume is diluent-independent. In this manner, we isolate the part of the extraction process that is

Table 3 The per-molecule DFT energy difference (ΔE) for a TMDGA molecule in a dimer or trimer compared to a TMDGA monomer. Results are shown for vacuum and implicit solvent models, as discussed in the text.

Solvent	ΔE_{Dimer} (kJ/mol)	ΔE_{Trimer} (kJ/mol)
Vacuum	-51.15	-47.07
n-Hexane	-40.56	-36.72
n-Dodecane	-41.95	-38.16
Benzene	-42.43	-38.67
Toluene	-39.82	-35.95

affected by the inert diluent from the metal-ligand binding that is not. Formation of the TODGA trimer can be broken down further as:

$$2\,\overline{\mathrm{TODGA}} \overset{K_2}{\rightleftharpoons} \overline{\mathrm{TODGA}_2} \tag{5}$$

$$\overline{\mathrm{TODGA}_2} + \overline{\mathrm{TODGA}} \overset{K_3}{\rightleftharpoons} \overline{\mathrm{TODGA}_3} \tag{6}$$

where Equation 5 and 6 are the step-wise formation of a TODGA monomer to dimer and then dimer to trimer complex, respectively. Given that K_2 and K_3 are equivalent, i.e., that TODGA association is isodesmic,[41] which will be demonstrated later, they can be labeled each as K_a, the association constant for adding an additional TODGA monomer to any TODGA complex of size n. Using the definition for distribution ratio established in Equation 1, this allows the following reorganization of the originally proposed K_{ex} in Equation 2:

$$\mathrm{K_{ex}} = \mathrm{K_T} \cdot \mathrm{K_M} = \mathrm{K_a}^2 \cdot \mathrm{K_M} = \frac{[\overline{\mathrm{TODGA}_3}]}{[\overline{TODGA}]^3} \cdot \frac{[\overline{TODGA_3M}]}{[\overline{TODGA}]^3[\mathrm{M}]} = \frac{\mathrm{D_M}}{[\overline{TODGA}]^3} \tag{7}$$

$$\mathrm{K_M} = \frac{\mathrm{D_M}}{\mathrm{K_a}^2[\overline{TODGA}]^3} \tag{8}$$

Given that we take K_M to be independent of the solvent, the relationship of TODGA extraction of metal M in two arbitrary solvents A and B can be expressed as:

$$\frac{\mathrm{D_{M\cdot A}}}{\mathrm{D_{M\cdot B}}} = \frac{{K_a}^2{}_A}{{K_a}^2{}_B}\frac{[\overline{TODGA}]^3_{\mathrm{A}}}{[\overline{TODGA}]^3_{\mathrm{B}}} \tag{9}$$

This is simplified to

$$\frac{\mathrm{D_{M\cdot A}}}{\mathrm{D_{M\cdot B}}} = \frac{{K_a}^2{}_A}{{K_a}^2{}_B} \tag{10}$$

for low metal concentration (where the TODGA concentration at equilibrium is unchanged by extraction) and assuming the Henry's law limit, where the activity coefficient of TODGA is taken to be unity. If this assumption does not hold, an analogous treatment with activities would yield a similar relationship between the assembly constants and distribution ratios. While D_M for a system can be measured from experiments, there remains a need to estimate K_a. For this, we use the O_c–O_c RDF maximum peak height. Since g(r) is a population analysis, the maximum peak height should directly correlate with the degree of pairwise TODGA self-association, and thus K_a.

The validity of this equilibrium constant methodology is demonstrated with Equation 10 using benzene as a "reference solvent." Additional comparisons are included, namely a pairwise cutoff sensitivity analysis between 6 and 8 Å (CN^2). From Figure 5a, it is evident that there are two features with minima located at 6 and 8 Å, though it is not clear if both of these structures should be considered as the first solvation interaction of O_c–O_c. Comparing ratios of D_{Am} with the RDF_{max} and coordination numbers from the O_c–O_c, this approach accurately captures the overall trends in distribution ratio between solvents solely using a pairwise analysis of TODGA self-association. In contrast to the DFT analyses discussed above that failed to exhibit correct trends between solvents, the MD methods with explicit solvent reasonably capture diluent effects on TODGA assembly. While the ratios for all pairwise quantities are in quantitative agreement, this simple initial analysis finds the correct order of magnitude, demonstrating potential predictive utility of pairwise analyses.

Table 4 Ratios of solvent descriptors with benzene as a baseline, i.e. the D_{Am} value shown below is ${D_{Am}}^{Solvent}/{D_{Am}}^{Benzene}$. D_{Am} is the solvent's Americium distribution ratio, RDF^2_{max} is the square of the O_C–O_C RDF maximum, and CN^2 6Å and CN^2 8Å are the O_C–O_C coordination number at 6 and 8 Å respectively.

Descriptor	n-Hexane	n-Dodecane	Toluene
D_{Am} (Exp)	84.6	76.9	0.770
RDF^2_{max} (MD)	58.5	59.2	0.917
CN^2 6Å (MD)	50.1	52.1	0.913
CN^2 8Å (MD)	34.9	30.2	0.950

3.3 Disruption of TODGA Structuring

Having demonstrated simple properties readily obtained from MD reasonably explain diluent effects, we now investigate the microstructure of these mixtures. In order to understand the underlying source of strong TODGA structuring, or lack thereof, in each solvent, spatial distribution functions (SDFs) are used to assess three-dimensional structuring. SDFs of O_c around the central TODGA ether group shown in Figure 6 show no obvious differences in TODGA–TODGA spatial structuring. This means that while the pairwise association energy of TODGA is significantly impacted in aromatic solvents, the overall way TODGA self-associates does not change between solvents and is not the source of unfavorable aggregation.

Without meaningful changes in the underlying mechanism TODGA self-structuring, it is possible that decreased TODGA self-association in aromatic solvents instead results from TODGA interacting differently with the solvent itself. This structuring is examined with RDFs of O_c and solvent carbons, Figure S4, and shows an expected strong anticorrelation of O_c–alkane structuring. Aromatics, however, exhibit some structure that, while below a value of 1, has a noticeable peak. Shifting the observed site from averaging all solvent carbons to specifically the aromatic ring center for benzene and toluene, the resultant RDF shown in Figure 7a has a structure that is well defined with a maximum value above one. Looking at the coordination number of solvent carbons and O_c atoms around the O_c site, Table 5, there are two to three times more aromatic than alkane carbons solvating the O_c site at 6.7 Å, with coordination number plots shown in Figure S2. This is directly contrasted by a five-fold reduction in O_c–O_c coordinations, implying that this preferential aromatic ring structuring around the TODGA head group is displacing other TODGA

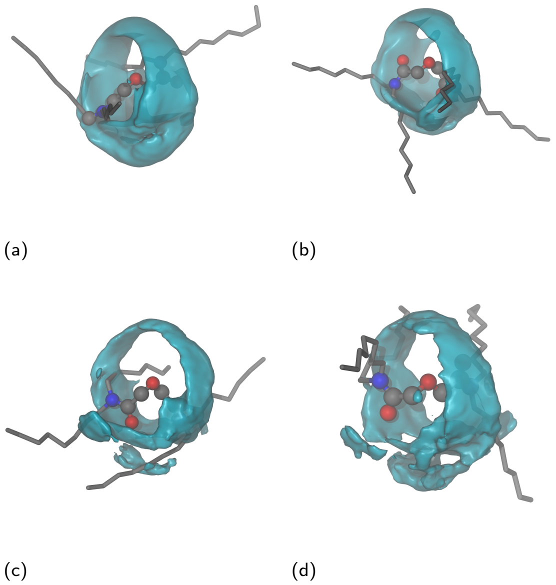
(a) (b)

(c) (d)

Fig. 6 Spatial distribution functions (SDFs) of TODGA etheric oxygen structuring around the central TODGA ether group in n-hexane (a), n-dodecane (b), benzene (c), and toluene (d). The green isosurface represents 20% of the max isodensity for the oxygen – oxygen pair in that particular solvent

molecules and preventing clustering.

Table 5 Coordination numbers of TODGA etheric oxygens (O_c) and solvent carbons (C_s) around a reference TODGA O_c site at 6.7 Å

Solvent	[TODGA] (mM)	O_c CN at 6.7 Å	C_s CN at 6.7 A
n-Hexane	200	1.17	10.9
n-Dodecane	200	1.15	14.0
Benzene	200	0.176	31.0
Toluene	200	0.170	30.1

The specificity of this aromatic center structure is better displayed with SDFs as well, and Figure 7b shows that both benzene and toluene preferentially coordinate the ether group predominantly above the O_c site, with some structuring below the etheric carbons as well. Figure S12 shows that no such structure occurs for any isodensity value for the linear alkanes and simply indicates a random distribution of carbon sites. All displayed isovalues are included in Table S2. It is clear with these pairwise analyses that aromatic solvents can preferentially solvate the DGA group in TODGA which is likely the source of the energy barrier and shallow energy minima seen in Figure 5b.

3.4 Graph Theoretic Cluster Analysis

While RDFs provide a great way to assess pairwise interactions, a full understanding of clustering behavior requires different methodology. Graph theoretic analysis provides a way to decompose the three dimensional distribution of O_c atoms into a collection of nodes and edges, where each node represents a single TODGA molecule and each edge is a connection between TODGAs if they are adjacent in solution. Each O_c node is connected by an edge to another O_c node if within a cutoff distance of 6 Å, determined from the first solvation shell in the RDFs shown in Figure 5a. Clusters are then defined as connected components of the resulting graph: collections of nodes that are connected through some path composed of edges, but are not connected through any path to any nodes not in the cluster. An example of a 5-mer DGA cluster and the resultant graph is provided in Figure 8. The cutoff was chosen after a sensitivity analysis to ensure that cluster behavior accurately represented truly clustering TODGA monomers. Too low of a cutoff results in clustering behavior capturing only very close-range interactions, flattening out any differences between solvents, while too large a cutoff results in excessive grouping of non-interacting TODGA monomers. Example results of an 8 Å cutoff showing this second effect as well as additional 6 Å analyses are included in Figures S5 - S11 which captures effects of the second peak rather than just the primary RDF peak, and validity of excluding the secondary will be demonstrated with some later results. All further discussed analysis is based on a 6 Å cutoff unless otherwise specified. The resultant collection of nodes and edges for each trajectory snapshot provides a simplified graph to be analyzed for various clustering metrics that are more easily accessible than traditional 3-dimensional, fully atomistic analyses.

First, cluster size distributions show a mostly linear reduction in cluster occurrence with increasing cluster size on a semi-log plot for clusters of size 3 and below. Exponential decay implies that the energy required to add an additional TODGA molecule to a cluster does not change with cluster size and is seen at lower cluster sizes for both varied solvents and varied concentrations, Figures 9a and 9b respectively. This cluster analysis validates the isodemsmic assumption for simplifying Equations 5 6 by showing that going from a TODGA monomer to a dimer and a dimer to a trimer are energetically equivalent. Furthermore, for higher concentrations of TODGA, it appears that the linearity of the distribution is preserved for greater cluster sizes. While this may be important for some systems, given that TODGA trimers are the relevant size for metal extraction, the drop off at larger cluster sizes for lower concentrations is less relevant for this particular study. Figure 9b again shows the saturation effect seen in the coordination numbers, where past 200 mM, the slope for sub 5-mers effectively overlap each other with similar cluster addition energetics. Solvent has an obvious effect on cluster formation at 200 mM TODGA, with aromatic clusters having a sharp decrease in cluster occurrence with greater size and no observable clusters above 5 and 6-mers. n-Hexane and n-dodecane show considerable clustering up to size 7 with similar energetics. Furthermore, the energetics implied by the solvent slopes match well with those shown in Figure 5b with the linear alkanes having a lower energy penalty with each additional cluster as compared to the aromatics and each solvent type having relatively similar energies of cluster formation. This demonstrates that the pairwise energies from RDFs in explicit, 3-dimensional space agree well with cluster formation in a simplified graph theoretic description.

In graph theory, the topology of a cluster is an important feature given the variety of possible cluster morphologies. Clustering coefficients (CC) provide a way of assessing degree of connection through observing all triplets in a graph, where a triplet is de-

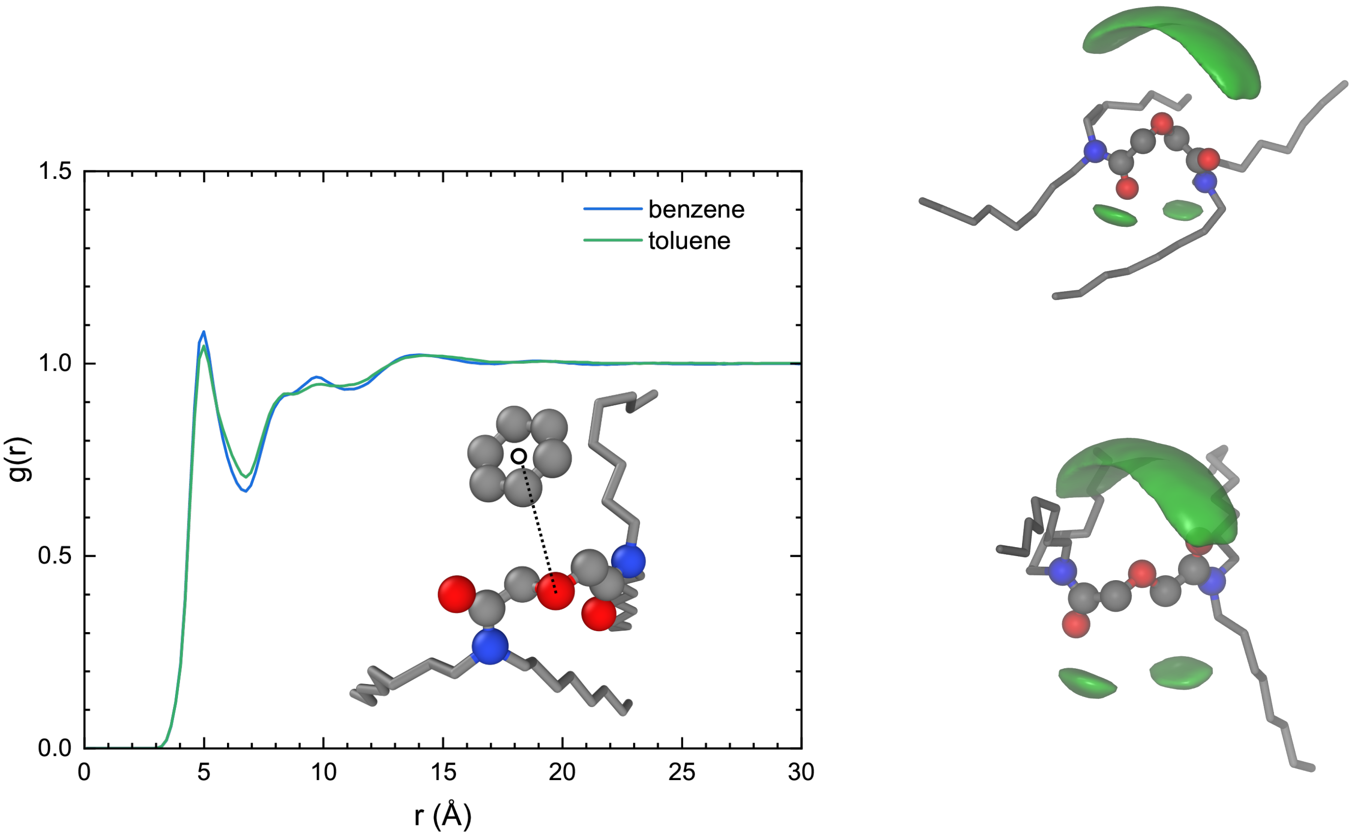

(a)

(b)

Fig. 7 Radial distribution function of TODGA etheric oxygen to the solvent ring center of benzene and toluene. An example of TODGA and Benzene is included for reference (a). SDFs of solvent carbon ring-center structuring around the central TODGA ether group in benzene (top) and toluene (bottom).

fined as any set of three nodes connected together. These triplets can exist as independent clusters of size three or be a subset of a larger cluster. For a given triplet, if all three points are within the cutoff to form a closed "triangle" it is assigned a value of 1, and if not it is considered open with a value of 0. When averaged over all triplets within a given cluster, it describes how interconnected that cluster's nodes are on a scale from zero to one. The value for a TODGA extraction system is immediately apparent, given that the extraction mechanism involves three DGA groups per metal extracted. A higher CC, and thus a higher percent of DGA triplets that are within close proximity of each other, would imply a solvent-ligand system where the ligands naturally and preferentially associate in an extraction-ready cluster.

This CC can be analyzed on a cluster size basis, yielding CC distributions as seen in Figures S5 and S6, and can indicate if there are significant deviations in CC based on cluster size. Such deviations are not seen as a concentration effect or with the two alkane solvents which indicate some deviation around an average value, but a noticeable decrease is seen for the aromatics. This is likely due to the extremely weak interaction of O_c in benzene and toluene, resulting in more difficult formation of interconnected clusters for each larger cluster. The system-wide, average CC value can be calculated by simply calculating the CC for all triplets in the system as well. This single value can then be used to easily compare degree of TODGA clustering connection from system to system. This is shown in Figure 10 as a concentration effect and solvent effect. Plotted alongside the CC is proportion of TODGA molecules participating in a cluster size of 3 or greater. This is similarly important, as CC is only relevant for triplets, so the proportion of TODGA participating in clusters of at least size 3 demonstrates what portion of the TODGA population the CC assesses.

Figure 10a indicates that as a concentration effect in n-dodecane, CC starts at roughly 0.26 at 100 mM and decreases to an average 0.17 for 400 through 600 mM, while the proportion of trimer or greater TODGA participants monotonically increase with concentration. This implies that cluster morphology changes from 100 to 400 mM TODGA in n-dodecane before reaching a stable CC for 400 through 600 mM. A possible explanation is that initial TODGA clusters form denser, more interconnected graphs that become less so as additional monomers are incorporated at the outer nodes of the graph with higher concentrations before reaching a final, high-concentration morphology.

At 200 mM, n-hexane and n-dodecane have a CC of 0.26 and

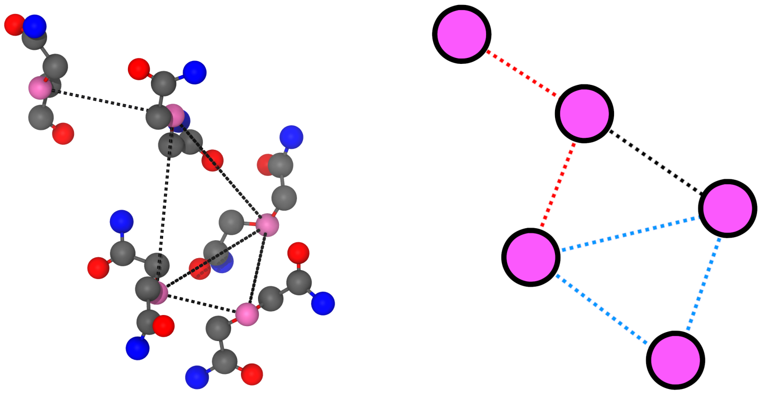

Fig. 8 A render of a DGA 5-mer cluster with lines drawn between the pink O_c atoms that satisfy a sub-6 Å distance cutoff. A 2-D representation of the resultant graph is shown with pink nodes and dashed edges. The red and blue dashes indicate example open and closed triplets, respectively. For reference, the example cluster has a total of four open triplets and two closed triplets

0.27, respectively, while benzene and toluene are lower at 0.29 and 0.19 respectively. This implies that using the primary 4.5 Å feature for graph analysis, triplet morphology is largely the same in all of these solvents. This isn't necessarily true for a larger edge definition, and is seen in plots S7. A key difference is an order-of-magnitude drop in TODGA monomers participating in larger clusters. Benzene and toluene have more than 95% of TODGA molecules existing as unconnected nodes, meaning they are considered free monomers. This may indicate that the physical interpretation of a closed triplet may be less relevant to extraction efficiency than propensity to form larger clusters, something that could potentially be inferred from the initial pairwise data. A clustering descriptor that can provide additional information is the fractal dimension D_f,[77–79] which is a power law fit to the radius of gyration as a function of cluster size. The results of this fit are included in the next section, and an in depth discussion is provided in the SI. Overall, the cluster analysis shows that aromatic solvents form significantly less clusters than aliphatic solvents, and when they do, the topology is less interconnected, as would be needed for efficient trivalent metal extraction.

These descriptors are useful for understanding clustering morphology and can also be used for population analysis similar to Table 4. The average absolute number of closed triplets present in a solvent directly calculated and compared to distribution ratios. These values are not squared like the RDF_{max} or CN like before, as the number of closed triplets is the fully formed complex and does not need to pairwise associate.

Table 6 Ratios of solvent descriptors with benzene as a baseline, i.e. the D_{Am} value shown below is ${D_{Am}}^{Solvent}/{D_{Am}}^{Benzene}$. Comparison of the ratio of solvent Americium distribution ratio (D_{Am}) and the number of closed triplets (N CT) within that solvent for an edge cutoff of 6 or 8 Å

Descriptor	n-Hexane	n-Dodecane	Toluene
D_{Am} (Exp)	84.6	76.9	0.770
N CT 6Å (MD)	85.0	76.8	0.833
N CT 8Å (MD)	42.3	31.5	1.04

Results from graphs derived with a 6 and 8 Å cutoff are shown in Table 6, with the 8 Å results showing similar predictive power to results from Table 4 with accurate order of magnitude matching and absolute deviation by a factor of approximately 2. Using a 6 Å cutoff instead shows remarkable accuracy, effectively matching the extraction efficiency ratios for all three solvents. While the impressive agreement may result in part from some form of fortuitous error cancellation—this approach is a simplification in many ways of an actual extraction process—the physically motivated choice of close triplets in representing the actual extractant association process suggests this correlation is not incidental. This graph theory derived quantifier is the most accurate predictor of solvent extraction efficiency thus far addressed and shows incredible potential for assessing new ligand–solvent mixtures *in silico* for potential extraction efficiency.

3.5 Descriptor Correlation with Distribution Ratios

Whether experimentally, semiempirically, or computationally derived, descriptors that try to reduce complex solute-solvent systems into singular values can clearly have mixed success in correlating with a desired outcome. Properties like dielectric constant or solubility parameters are extremely valuable for describing systems for more direct or designed applications, but can struggle to appropriately correlate to phenomena that are more niche or outside of their original design. Furthermore, the thermodynamically critical steps of TODGA trimer assembly and trimer–metal coordination cannot be adequately described experimental properties that only describe the solvent alone, and not the solvent–ligand relationship. Figure 2 shows that while these experimental and semi-empirical parameters correlate somewhat with reported americium distribution ratios, there is poor grouping of the aromatics and alkanes. Looking at simulation-derived quantifiers in Figure 11, it is similarly evident that some descriptors do a better job of grouping data than others.

Pairwise interactions do remarkably well, with the maximum RDF peak and O_c–O_c coordination numbers tightly correlating the two different extraction regimes better than some more physically motivated clustering descriptors. Clustering coefficient and does

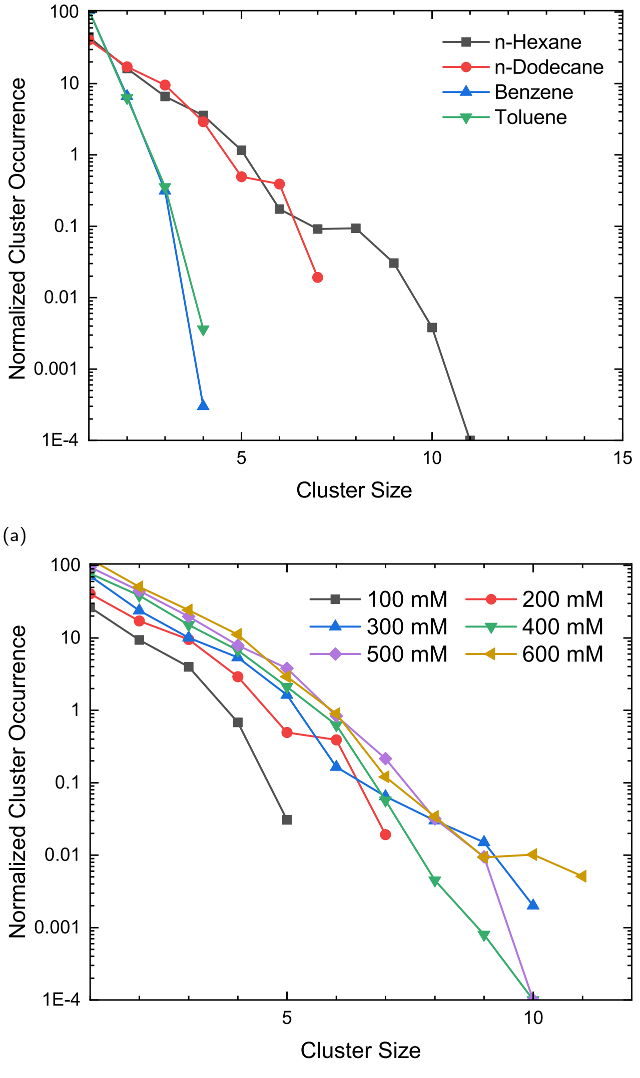

(a)

(b)

Fig. 9 Cluster size distributions of 200 mM TODGA in various solvents (a) and various concentrations of TODGA in n-dodecane (b) with an edge cutoff of 6 Å.

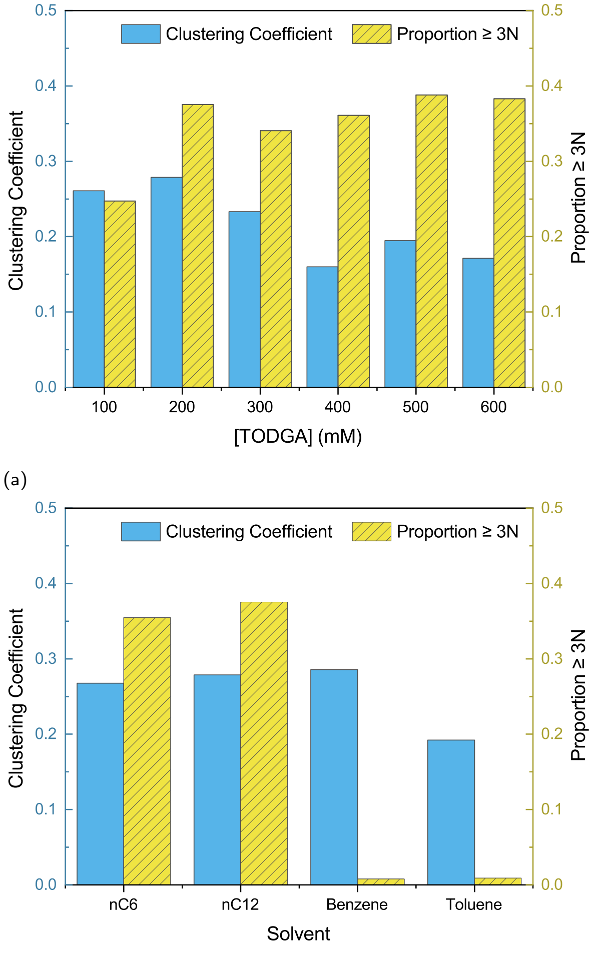

(a)

(b)

Fig. 10 Clustering coefficients and proportion of monomers participating in clusters of size 3 or greater for TODGA clusters as (a) a solvent effect at 200 mM TODGA and (b) a concentration effect of TODGA in pure n-dodecane.

somewhat well at 8 Å, but is clearly highly sensitive to the selected cutoff, and simply counting the total proportion of TODGA participating in larger clusters does the better regardless of cutoff chosen. Fractal dimension shows reasonable correlation, though this seems attributable more to systems with similar max cluster sizes having similar fractal dimension fits.

Overall, it is evident that the number of closed triplets at a 6 Å cutoff performed the best while also providing a physically justified conclusion: that the equilibrium “concentration” of closed triplets was directly predictive of relative extraction efficiency between diluents of americium with TODGA. The propensity of any two TODGA molecules to associate strongly, which is most directly captured by pairwise analysis, performed adequately well at predicting solvent extraction efficiency. Whether all of these observations extend to further solvents, especially solvent mixtures, remains to be seen in further studies given the sparseness of this initial test dataset. Yet in spite of this sparseness, the number of closed triplets and, to a lesser degree, the pairwise descriptors, correlate strongly with the impact of the selected inert diluents on metal distribution. Given the strong physical motivation for these specific properties, these results suggests a potentially predictive approach to understanding solvent effects that may be implemented for arbitrary solvent–ligand mixtures.

4 Conclusion

Ultimately, this study focused on understanding diluent effects in separations. In particular, we investigate how the diluent affects ligand assembly in solvent extraction of metal ions. Due to the lack of adequate experimental properties or parameters to correlate with solvent extraction efficiency, an alternative framework was proposed. By breaking down ligand–metal extraction complex formation into a solvent dependent and independent processes, solvent effects on ligand assembly, and thus extraction efficiency, could be investigated with molecular dynamics simulations of binary ligand–solvent mixtures.

Pairwise RDFs indicated that a significant loss in TODGA structuring in aromatic solvents resulted in poor association energet-

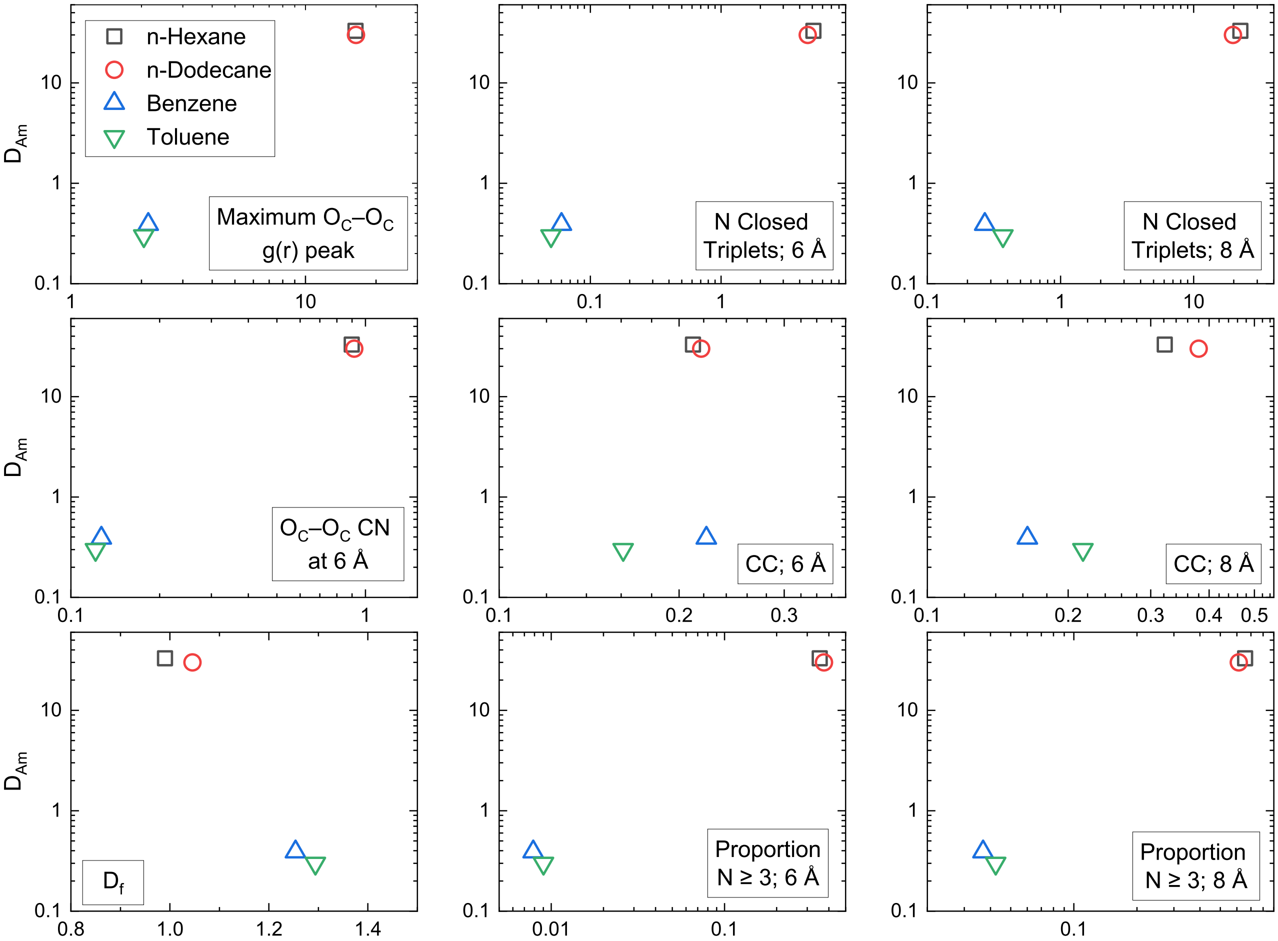

Fig. 11 Comparison of D_{Am} with simulation derived quantifiers. Top row: maximum peak height of O_c–O_c g(r), number of closed triplets with a 6 Å cutoff, and number of closed triplets with a 8 Å cutoff; Middle row: O_c–O_c coordination number at 6 Å, clustering coefficient with 6 Å cutoff, and clustering coefficient with 8 Å cutoff; Bottom row: fit fractal dimension with 8 Å cutoff, proportion of TODGA participating in size greater than 3 with a 6 Å cutoff, and the same proportion with an 8 Å cutoff. All values are from MD simulations of 200 mM TODGA in the solvents n-dodecane, n-hexane, benzene, and toluene.

ics, with shallow energy minima. An analysis using equilibrium constants provided a satisfying explanation for the orders of magnitude difference in the distribution ratios of americium in linear alkanes or aromatic solvents. SDFs showed the etheric oxygen of the TODGA molecule has a measurable solvation by the aromatic ring of benzene and toluene penalizing TODGA-TODGA association.

Graph theoretic analysis proved a powerful method for studying TODGA clusters, with size distributions indicating that additions of TODGA to existing clusters had a constant energy penalty at small cluster sizes. Furthermore, a reduction in cluster sizes between the alkanes and aromatics and a large decrease in closed-triplet clustering coefficients was observed. Aromatic complexes also had an order of magnitude smaller fraction of TODGA molecules participating in larger clusters, implying that the solvents are ill-suited to favorably assembling multiple TODGAs together for metal coordination.

Tying the pairwise and graph theory analyses together is a first-principles focus on equilibrium constants of the metal extraction process. Maximum RDF peaks and coordination numbers were moderately predictive of metal extraction efficiency, while graph-derived total closed triplet count showed nearly exact correlation with experimental distribution ratios. While this approach involving isolating energetic contributions of metal-free binary mixtures is a simplification to the actual extraction process, these findings demonstrate that simulation-derived descriptors may go beyond merely correlating with experimental data, potentially enabling prediction of differences ion extraction behavior imparted by inert diluents. Overall, these promising initial results with four exploratory solvents suggest MD simulations may be a robust method for assessing ligand–solvent mixtures, as this approach is easily scalable to new ligands or solvents. Further analysis of additional solvents and solvent mixtures will allow for confirmation whether these MD clustering descriptors can continue to accurately predict metal distribution ratios and even potentially provide guidance for selecting an ideal ligand-solvent system.

Author Contributions

Conceptualization: D.P. and M.J.S; Data Curation: D.P. and S.S.; Formal Analysis: D.P.; Funding Acquisition: M.J.S; Investigation: D.P. and M.J.S; Methodology: D.P. and M.J.S; Project Administration: M.J.S; Supervision: M.J.S; Validation: D.P.; Visualization:

D.P.; Writing – Original Draft: D.P.; Writing – Review & Editing: D.P. and M.J.S

Conflicts of interest

There are no conflicts of interest to declare.

Acknowledgements

This work was supported by U.S. Department of Energy (DOE), Office of Science, Office of Basic Energy Sciences, Chemical Sciences, Geosciences, and Biosciences Division, Separation Science Program, under Contract DE-AC02-06CH11357 to UChicago Argonne, LLC, Operator of Argonne National Laboratory. This research used resources of beamline 12-ID-C at the Advanced Photon Source, a U.S. DOE Office of Science User Facility, operated for the DOE Office of Science by Argonne National Laboratory under the same contract number. We gratefully acknowledge the computing resources provided on Bebop, a high-performance computing cluster operated by the Laboratory Computing Resource Center at Argonne National Laboratory.

Notes and references

1 R. K. Jyothi, T. Thenepalli, J. W. Ahn, P. K. Parhi, K. W. Chung and J. Y. Lee, *Journal of Cleaner Production*, 2020, **267**, 122048.

2 V. Balaram, *Geoscience Frontiers*, 2019, **10**, 1285–1303.

3 N. Dushyantha, N. Batapola, I. M. Ilankoon, S. Rohitha, R. Premasiri, B. Abeysinghe, N. Ratnayake and K. Dissanayake, *Ore Geology Reviews*, 2020, **122**, 103521.

4 N. Swain and S. Mishra, *Journal of Cleaner Production*, 2019, **220**, 884–898.

5 L. Grandell and M. Höök, *Sustainability (Switzerland)*, 2015, **7**, 11818–11837.

6 A. Jordens, Y. P. Cheng and K. E. Waters, *Minerals Engineering*, 2013, **41**, 97–114.

7 Z. Zhu, Y. Pranolo and C. Y. Cheng, *Minerals Engineering*, 2015, **77**, 185–196.

8 M. K. Jha, A. Kumari, R. Panda, J. Rajesh Kumar, K. Yoo and J. Y. Lee, *Hydrometallurgy*, 2016, **165**, 2–26.

9 G. R. Choppin and A. Morgenstern, *Solvent Extraction and Ion Exchange*, 2000, **18**, 1029–1049.

10 F. Xie, T. A. Zhang, D. Dreisinger and F. Doyle, *Minerals Engineering*, 2014, **56**, 10–28.

11 A. M. Wilson, P. J. Bailey, P. A. Tasker, J. R. Turkington, R. A. Grant and J. B. Love, *Chemical Society Reviews*, 2014, **43**, 123–134.

12 E. O. Opare, E. Struhs and A. Mirkouei, *Renewable and Sustainable Energy Reviews*, 2021, **143**, 110917.

13 V. S. Kislik, in *Solvent Extraction*, ed. V. S. Kislik, Elsevier, Amsterdam, 2012, pp. 3–67.

14 M. S. Tyumentsev, M. R. J. Foreman, C. Ekberg, A. V. Matyskin, T. Retegan and B. M. Steenari, *Hydrometallurgy*, 2016, **164**, 24–30.

15 A. Leoncini, J. Huskens and W. Verboom, *Chemical Society Reviews*, 2017, **46**, 7229–7273.

16 D. Whittaker, A. Geist, G. Modolo, R. Taylor, M. Sarsfield and A. Wilden, *Solvent Extraction and Ion Exchange*, 2018, **36**, 223–256.

17 A. Geist and P. J. Panak, *Solvent Extraction and Ion Exchange*, 2021, **39**, 128–151.

18 A. A. Peroutka, S. S. Galley and J. C. Shafer, *Coordination Chemistry Reviews*, 2023, **482**, 215071.

19 A. Turanov, V. Karandashev and M. Boltoeva, *Hydrometallurgy*, 2020, **195**, 105367.

20 R. Poirot, X. Le Goff, O. Diat, D. Bourgeois and D. Meyer, *ChemPhysChem*, 2016, **17**, 2112–2117.

21 Y. Marcus, *Solvent Extraction and Ion Exchange*, 1989, **7**, 567–575.

22 T. Sato, T. Nakamura and M. Kuwaiiara, *Solvent Extraction and Ion Exchange*, 1985, **3**, 283–307.

23 S. A. Ansari, P. Pathak, P. K. Mohapatra and V. K. Manchanda, *Chemical Reviews*, 2012, **112**, 1751–1772.

24 A. F. Barton, *Chemical Reviews*, 1975, **75**, 731–753.

25 S. A. Ansari, P. Pathak, P. K. Mohapatra and V. K. Manchanda, *Chemical reviews*, 2012, **112**, 1751–1772.

26 T. V. Healy, *Journal of Inorganic and Nuclear Chemistry*, 1961, **19**, 328–339.

27 M. Regadío, N. K. Batchu and K. Binnemans, *Chemical Engineering Research and Design*, 2020, **161**, 304–311.

28 A. F. Barton, *Chemical Reviews*, 1975, **75**, 731–753.

29 R. Poirot, X. Le Goff, O. Diat, D. Bourgeois and D. Meyer, *ChemPhysChem*, 2016, 2112–2117.

30 S. M. Ali, S. Pahan, A. Bhattacharyya and P. K. Mohapatra, *Physical Chemistry Chemical Physics*, 2016, **18**, 9816–9828.

31 P. Ivanov, J. Mu, L. Leay, C. Sharrad and A. Masters, *Solvent Extraction and Ion Exchange*, 2017, **35**, 251–265.

32 P. Ren, C. Z. Wang, W. Q. Tao, X. F. Yang, S. L. Yang, L. Y. Yuan, Z. F. Chai and W. Q. Shi, *Inorganic Chemistry*, 2020, **59**, 14218–14228.

33 M. Špadina, J.-F. Dufrêche, S. Pellet-Rostaing, S. Marčelja and T. Zemb, *Langmuir*, 2021, **37**, 10637–10656.

34 Y. Sasaki, Y. Sugo, S. Suzuki and T. Kimura, *Analytica Chimica Acta*, 2005, **543**, 31–37.

35 S. A. Ansari, P. Pathak, P. K. Mohapatra and V. K. Manchanda, *Separation and Purification Reviews*, 2011, **40**, 43–76.

36 Y. Sasaki, Y. Sugo, S. Suzuki and S. Tachimori, *Solvent Extraction and Ion Exchange*, 2001, **19**, 91–103.

37 J. N. Sharma, R. Ruhela, K. N. Harindaran, S. L. Mishra, S. K. Tangri and A. K. Suri, *Journal of Radioanalytical and Nuclear Chemistry*, 2008, **278**, 173–177.

38 M. Hirata, P. Guilbaud, M. Dobler and S. Tachimori, *Physical Chemistry Chemical Physics*, 2003, **5**, 691–695.

39 M. B. Singh, A. J. Mukhtyar, Y. Z. Bootwala and V. G. Gaikar, *Separation Science and Technology (Philadelphia)*, 2017, **52**, 1172–1185.

40 B. Sadhu and A. E. Clark, *Journal of Molecular Liquids*, 2022, **359**, 119226.

41 D. Massey, A. Masters, J. Macdonald-Taylor, D. Woodhead and R. Taylor, *Journal of Physical Chemistry B*, 2022, **126**, 6290–

6300.

42 A. G. Baldwin, A. S. Ivanov, N. J. Williams, R. J. Ellis, B. A. Moyer, V. S. Bryantsev and J. C. Shafer, *ACS Central Science*, 2018, **4**, 739–747.

43 D. Stamberga, M. R. Healy, V. S. Bryantsev, C. Albisser, Y. Karslyan, B. Reinhart, A. Paulenova, M. Foster, I. Popovs, K. Lyon, B. A. Moyer and S. Jansone-Popova, *Inorganic Chemistry*, 2020, **59**, 17620–17630.

44 A. Kimberlin, D. Guillaumont, S. Arpigny, B. Camès, P. Guilbaud, G. Saint-Louis, H. Galán and L. Berthon, *New Journal of Chemistry*, 2021, **45**, 12479–12493.

45 L. Berthon, A. Paquet, G. Saint-Louis and P. Guilbaud, *Solvent Extraction and Ion Exchange*, 2021, **39**, 204–232.

46 K. R. Swami, K. A. Venkatesan, P. Sahu and S. M. Ali, *Journal of Molecular Structure*, 2020, **1221**, 128795.

47 S. Seifert, R. E. Winans, D. M. Tiede and P. Thiyagarajan, *J. Appl. Crystallogr.*, 2000, 782–784.

48 C. A. Dreiss, K. S. Jack and A. P. Parker, *Journal of applied crystallography*, 2006, **39**, 32–38.

49 P. Bauer, B. Hess and E. Lindahl, *GROMACS 2022.1 Manual*, 2022, `https://doi.org/10.5281/zenodo.6451567`.

50 J. M. Wang, D. A. Case, R. M. Wolf, J. W. Caldwell and P. A. Kollman, *Journal of Computational Chemistry*, 2004, **25**, 1157–1174.

51 Q. N. Vo, C. Hawkins, L. X. Dang, M. Nilsson and H. D. Nguyen, *J. Phys. Chem. B*, 2015, **119**, 1588–1597.

52 M. J. Frisch, G. W. Trucks, H. B. Schlegel, G. E. Scuseria, M. A. Robb, J. R. Cheeseman, G. Scalmani, V. Barone, G. A. Petersson, H. Nakatsuji, X. Li, M. Caricato, A. V. Marenich, J. Bloino, B. G. Janesko, R. Gomperts, B. Mennucci, H. P. Hratchian, J. V. Ortiz, A. F. Izmaylov, J. L. Sonnenberg, D. Williams-Young, F. Ding, F. Lipparini, F. Egidi, J. Goings, B. Peng, A. Petrone, T. Henderson, D. Ranasinghe, V. G. Zakrzewski, J. Gao, N. Rega, G. Zheng, W. Liang, M. Hada, M. Ehara, K. Toyota, R. Fukuda, J. Hasegawa, M. Ishida, T. Nakajima, Y. Honda, O. Kitao, H. Nakai, T. Vreven, K. Throssell, J. A. Montgomery Jr., J. E. Peralta, F. Ogliaro, M. J. Bearpark, J. J. Heyd, E. N. Brothers, K. N. Kudin, V. N. Staroverov, T. A. Keith, R. Kobayashi, J. Normand, K. Raghavachari, A. P. Rendell, J. C. Burant, S. S. Iyengar, J. Tomasi, M. Cossi, J. M. Millam, M. Klene, C. Adamo, R. Cammi, J. W. Ochterski, R. L. Martin, K. Morokuma, O. Farkas, J. B. Foresman and D. J. Fox, *Gaussian~16 {R}evision {C}.01*, 2016.

53 A. D. Becke, *Physical Review A*, 1988, **38**, 3098–30100.

54 A.-r. Allouche, *Journal of computational chemistry*, 2012, **32**, 174–182.

55 A. Jakalian, D. B. Jack and C. I. Bayly, *Journal of computational chemistry*, 2002, **23**, 1623–1641.

56 J. Wang, W. Wang, P. A. Kollman and D. A. Case, *Journal of Molecular Graphics and Modelling*, 2006, **25**, 247–260.

57 L. Martínez, R. Andrade, E. G. Birgin and J. M. Martínez, *Journal of Computational Chemistry*, 2009, **30**, 2157–2164.

58 M. Brehm, M. Thomas, S. Gehrke and B. Kirchner, *The Journal of Chemical Physics*, 2020, **152**, 164105.

59 M. Brehm and B. Kirchner, *Journal of Chemical Information and Modeling*, 2011, **51**, 2007–2023.

60 H. Liu and S. J. Paddison, *Physical Chemistry Chemical Physics*, 2016, **18**, 11000–11007.

61 A. A. Hagberg, D. A. Schult and P. J. Swart, *7th Python in Science Conference (SciPy 2008)*, 2008, 11–15.

62 A. Stukowski, *Modelling and Simulation in Materials Science and Engineering*, 2010, **18**,.

63 W. Humphrey, A. Dalke and K. Schulten, *Journal of molecular graphics*, 1996, **14**, 33–38.

64 J. Ravi, S. Mishra, R. Murali and N. D. N. K. Pandey, *Journal of Radioanalytical and Nuclear Chemistry*, 2021, **328**, 1301–1312.

65 J. Troncoso, D. Bessières, C. A. Cerdeiriña, E. Carballo and L. Romaní, *Fluid Phase Equilibria*, 2003, **208**, 141–154.

66 M. A. Rivas, S. M. Pereira, N. Banerji and T. P. Iglesias, *Journal of Chemical Thermodynamics*, 2004, **36**, 183–191.

67 Y. Huo, S. Xia and P. Ma, *Journal of Chemical and Engineering Data*, 2007, **52**, 2077–2082.

68 S. Enders, H. Kahl and J. Winkelmann, *Journal of Chemical and Engineering Data*, 2007, **52**, 1072–1079.

69 T. Inagaki, S. Aono, H. Nakano and T. Yamamoto, *The Journal of Physical Chemistry B*, 2014, **118**, 5499–5508.

70 M. Vazdar, J. Heyda, P. E. Mason, G. Tesei, C. Allolio, M. Lund and P. Jungwirth, *Accounts of Chemical Research*, 2018, **51**, 1455–1464.

71 I. G. Shenderovich, *Molecules*, 2019, **24**, year.

72 S. E. Kruchinin and M. V. Fedotova, *The Journal of Physical Chemistry B*, 2021, **125**, 11219–11231.

73 A. V. Shishkina, A. A. Ksenofontov, N. V. Penkov and M. V. Vener, *Molecules*, 2022, **27**, year.

74 Y. Bai, A. Gong, L. Qiu, Y. Wang, G. Gao, W. Zhao, Y. Liu, J. Yin, X. Huang and Y. Chen, *Separations*, 2024, **11**, year.

75 T. Prathibha, S. Kumar, S. Chandra, S. Maji and N. Ramanathan, *Inorganica Chimica Acta*, 2023, **548**, 121396.

76 G. P. Horne, C. A. Zarzana, C. Rae, A. R. Cook, S. P. Mezyk, P. R. Zalupski, A. Wilden and B. J. Mincher, *Phys. Chem. Chem. Phys.*, 2020, **22**, 24978–24985.

77 L. Dougan, S. P. Bates, R. Hargreaves, J. P. Fox, J. Crain, J. L. Finney, V. Réat and A. K. Soper, *Journal of Chemical Physics*, 2004, **121**, 6456–6462.

78 A. Oleinikova, I. Brovchenko, A. Geiger and B. Guillot, *Journal of Chemical Physics*, 2002, **117**, 3296–3304.

79 L. Pártay, P. Jedlovszky, I. Brovchenko and A. Oleinikova, *Physical Chemistry and Chemical Physics*, 2007, **9**, 1341–1346.